Revealing Electrolytic Ion Sorption in Layered Graphene Galleries through Low-Temperature Solid-State NMR

Daniel Lee, Harish Banda, Sandy Périé, Coralie Marcucci, Yves Chenavier, Lionel Dubois, Pierre-Louis Taberna, Patrice Simon, Gaël de Paëpe, Florence Duclairoir

▶ **To cite this version:**

Daniel Lee, Harish Banda, Sandy Périé, Coralie Marcucci, Yves Chenavier, et al.. Revealing Electrolytic Ion Sorption in Layered Graphene Galleries through Low-Temperature Solid-State NMR. Chemistry of Materials, 2023, 35 (10), pp.3841-3848. 10.1021/acs.chemmater.2c03502 . hal-04250917

HAL Id: hal-04250917
https://hal.science/hal-04250917

Submitted on 23 Oct 2023

HAL is a multi-disciplinary open access archive for the deposit and dissemination of scientific research documents, whether they are published or not. The documents may come from teaching and research institutions in France or abroad, or from public or private research centers.

L'archive ouverte pluridisciplinaire **HAL**, est destinée au dépôt et à la diffusion de documents scientifiques de niveau recherche, publiés ou non, émanant des établissements d'enseignement et de recherche français ou étrangers, des laboratoires publics ou privés.

Revealing electrolytic ion-sorption in layered graphene galleries through low temperature solid-state NMR

Daniel Lee,[a #†] *Harish Banda,*[b‡†] *Sandy Périé,*[b] *Coralie Marcucci,*[b] *Yves Chenavier,*[b] *Lionel Dubois,*[b] *Pierre-Louis Taberna,*[cd] *Patrice Simon,*[cd] *Gaël De Paëpe**[a] *and Florence Duclairoir**[b]

[a]Université Grenoble Alpes, CEA, IRIG-MEM, Grenoble 38000, France

[b]Université Grenoble Alpes, CEA, CNRS, IRIG-SyMMES, Grenoble 38000, France

[c]CIRIMAT, Université de Toulouse, CNRS, INPT, UPS, Toulouse 31062, France

[d]Réseau sur le Stockage Electrochimique de l'Energie (RS2E), CNRS FR3459, Amiens 80039, France

[†]These authors contributed equally

KEYWORDS: Supercapacitors, pillared graphene materials, low-temperature solid state NMR, ion sieving

ABSTRACT

There is an ever-growing desire to use and store energy from sustainable resources. Pillared graphene materials offer high capacitive performances in supercapacitors, presumably through enhanced electrolytic ion sorption in their chemically-engineered inter-layer graphene galleries. Herein, a judicious combination of the removal of excess electrolyte, isotopic-enrichment of the pillar molecules, and the use of low temperatures (100 K) enables solid-state NMR spectroscopy to efficiently probe nuclear spin polarization exchange between the electrolyte and the electrode. This provides the direct detection of electrolyte ions in proximity to the gallery pillars, evidencing the adsorption of ions in such two-dimensional galleries. However, when the ions are larger than the gallery d-spacing they are not observed to enter the galleries and total storage capacity is accordingly reduced. This methodology provides a means to locate electrolyte ions upon charging or discharging devices and thus will be invaluable in the quest for the design of materials with vastly improved power densities.

INTRODUCTION

The ever-increasing demand for clean and reliable energy in mobile applications calls for the development of efficient energy storage devices. Among various electrochemical devices, supercapacitors (SCs) have emerged as excellent candidates that can handle rapid charge and discharge processes over millions of cycles. SCs consist of two porous electrodes that are immersed in an electrolytic solution and are separated by an ion-permeable membrane. Upon polarization of the electrodes, ions in the electrolyte form an electric double layer of opposite

polarity and offer reliable charge-storage. In order to maximize the charge stored, nano-porous materials with high specific surface areas, such as activated carbons and carbide-derived carbons, are often used as electrodes.[1–4] With increasing demand for enhanced energy storage capabilities in SCs, other carbon-based materials, such as onion-like carbon[5], carbon nanotubes[6], and graphene[7], are extensively studied. In this context, graphene-based materials are potential candidates for SCs owing to the excellent electrical conductivity and high theoretical capacitance of 550 F/g offered by graphene.[8] However, spontaneous restacking of graphene sheets due to π-π interactions has led to experimental capacitances well below this theoretical capacitance, achieved in the range of 100 F/g for reduced graphene oxide (RGO), a graphene-like material.[9] Recently, pillared graphene materials have emerged as a new class of materials that prevent spontaneous restacking of individual graphene sheets by separating them with a chemical linker.[10–16] Among different approaches, the strategy to use graphene oxide as the precursor and alkyl diamines as chemical pillars has offered facile synthetic and design control.[17–19] Alkyl diamines bridge graphene sheets through covalent and non-covalent interactions and offer a robust pillared-graphene architecture with chemically-engineered "galleries" available for ion sorption in SCs.[16–18] An ion-sieving study using cations of varied sizes provided an indirect evidence for ion-sorption inside the 2D galleries, wherein cations smaller than the inter-layer spacing deliver enhanced capacitances.[17,20] In addition, lowering the number of pillars inside the 2D galleries was also shown improve ion transport characteristics in SCs.[21] Together, these findings present the idea of ion sorption inside the 2D galleries as an avenue towards achieving

enhanced capacitances in graphene-based materials. Nevertheless, atomic-scale information on ion-sorption inside the 2D galleries is still lacking and is necessary to further understand ion sorption mechanisms in these materials.

Solid-state nuclear magnetic resonance (ssNMR) spectroscopy has proved to be a powerful tool for direct characterization of ion sorption in SCs from in-situ[22–25] and ex-situ studies.[26–30] The investigation of ion-sorption in electrode micropores through soaking in increasing amounts of electrolyte has allowed for decisive differentiation of ion sorption sites.[24,27] This is possible because the chemical environment of ion/solvent is directly related to the NMR chemical shift and that adsorbed species on microporous graphitic materials undergo specific shifts due to ring-current effects.[31] The strength of NMR experiments is thus to allow differentiating ions/solvent molecules that are present inside the pores (in-pore) from the ones lying outside the pore (ex-pore).[27,30] For instance, ex-situ studies by Deschamps et al. have analysed the relative concentrations of anions, cations and solvents in “in-pore” and “ex-pore” sites and identified a strong influence of the nature of porous carbon on electrolyte reorganization upon polarization.[27] Extensive in-situ studies by Grey and co-workers on various carbons have provided substantial insight into ion dynamics during charge-discharge processes.[23,32,33] Another study of a graphene film in SCs, using ex-situ ssNMR, found two distinct processes of co-ion expulsion and counter-ion adsorption upon polarization.[34]

Herein, we show that ssNMR under low temperature (LT) magic angle spinning (MAS) conditions is a powerful approach to study ion-sorption in the 2D galleries of a state-of-the-art pillared graphene material (6-GH). A washing procedure, similar to that of Deschamps et al.,[27] reveals signals from adsorbed species and the use of low temperatures limits residual motion of the adsorbed species, enabling improved nuclear polarization transfer. This, combined with MAS conditions, provides the necessary high resolution and sensitivity for detailed investigations of the adsorbed species in the in-pore regions of this complex system. In this work, we use polarization transfer from nuclei in the pillars to receptive ^{31}P nuclei in purposefully-selected phosphonium electrolyte ions to probe the presence of these ions inside the chemically-engineered graphene galleries. This methodology, along with the ion-sieving property of the 2D galleries confirmed through an electrochemical study of electrolyte cations with varied sizes, revealed the presence of cations between the graphene sheets. This approach provides direct information about ion sorption in pillared materials and will thus help further optimize such materials towards high-energy SCs.

EXPERIMENTAL METHODS

Material Synthesis

Graphene oxide (GO) was synthesized following procedures reported elsewhere.[21] Pillared graphene hydrogels (6-GHs) were synthesized using a mixture of 5 ml of aqueous GO (5 mg/ml) solution and 32.5 mg of 1.6-hexanediamine (^{15}N-labelled) pillar molecule (Fig. 1a). The reaction mixture was sonicated for 10 min, transferred into a 23 ml Teflon vessel and heated at 180^{o}C for

17 h. The resulting hydrogel was cleaned with excess ethanol and water sequentially, and freeze-dried (sample freezing was carried out using liquid N_2) to obtain 6-GH aerogels.

Electrochemical tests

The synthesized aerogels were tested in a three-electrode supercapacitor configuration (Fig. S1) with porous carbon (YP50) as counter and silver wire as pseudo-reference electrodes, respectively. A 25 μm thick cellulose sheet served as a separator. The working electrodes were fabricated as a slurry by mixing active materials, polyvinylidene fluoride (PVDF), and acetylene black carbon in a ratio of 80:10:10 using N-methyl-2-pyrrolidone and were coated onto 0.5 cm^2 stainless steel disks. The as-prepared electrodes were dried at 65 ^oC in air for 3 h prior to drying under vacuum at 120 ^oC overnight. The dried electrodes had an active mass loading of 2-3 $mg.cm^{-2}$. 1 M Tetralkylphosponium tetrafluoroborate ($TAPBF_4$) salt solutions in anhydrous acetonitrile (ACN) with varying cation sizes; ethyl ($TEPBF_4$) – 0.68 nm, butyl ($TBPBF_4$) – 0.82 nm and octyl ($TOPBF_4$) – 1.12 nm were used as electrolytes. $TEPBF_4$ and $TBPBF_4$ were purchased from TCI. $TOPBF_4$ was prepared through an ion-exchange procedure between TOPBr (purchased from TCI) and $NaBF_4$ in a mixture of ACN/acetone (50:50). A multichannel VMP3 potentiostat with EC-Lab software (Biologic) was used for all electrochemical studies.

ssNMR experimental techniques

Conventional and DNP-enhanced solid-state nuclear magnetic resonance (ssNMR) spectroscopy were performed using a Bruker AVIII 9.4 T 263 GHz / 400 MHz DNP-NMR

spectrometer equipped with a 3.2 mm low-temperature-capable magic angle sample spinning (MAS) probe. DNP was not attempted for the pillared materials due to the known challenges with hyperpolarizing conductive materials.[35] Here, instead, we show the usefulness of low-temperature measurements. All experiments were performed using cryogenic nitrogen gas to cool and spin the sample at 100 K with a MAS frequency of 8 kHz unless otherwise specified. The sample temperature was externally calibrated using the T_1 of ^{79}Br in KBr.[36] $\{^1$H-$\}^{31}$P and $\{^1$H-$\}^{15}$N cross-polarization (CP)MAS NMR experiments were recorded using 100 kHz nutation for ^{1}H $\pi/2$ pulses and 65 kHz for ^{1}H heteronuclear continuous wave decoupling, a ramped (50-100%) power to match a Hartmann-Hahn CP condition when using 50 kHz for ^{31}P or 36 kHz ^{15}N nutation during 1 ms CP spin-locking and using a spin-echo of one rotor period total duration (50 kHz for ^{31}P or 36 kHz ^{15}N π-pulses) before free-induction decay (FID) acquisition. Between 444 and 8192 and 444 and 1664 transients were recorded for the $\{^1$H-$\}^{31}$P and $\{^1$H-$\}^{15}$N CPMAS experiments, respectively, using a recycle delay of ~1 s between transients and 50 Hz exponential apodization before Fourier transformation of the FID. The 2D *z*-filtered TEDOR ^{15}N–^{31}P dipolar correlation spectrum of 6-GH was recorded with a starting $\{^1$H-$\}^{31}$P CP step of 0.5 ms, 7 ms total TEDOR mixing, 2048 transients for each of 6 complex (States-TPPI) t_1 increments of 123.3 μs, using a recycle delay of ~1 s between transients and 300 and 50 Hz exponential apodization in the direct and indirect dimensions, respectively, before double Fourier transform.[37] For the 1D $\{^{15}$N-$\}^{31}$P *z*-filtered TEDOR experiments of 6-GH with various electrolytes, 7, 14, or 20 ms total TEDOR mixing (as stated) was employed for up to 10240

transients. The other parameters were as for the 2D version. For the DNP-enhanced 2D ^{15}N–^{31}P *z*-filtered TEDOR experiment of 25 mM guanosine-$^{15}N_5$ 5'-monophosphate sodium salt solution (GMP), a starting $\{^{1}H-\}^{31}P$ CP step of 2.25 ms and a 7 ms total TEDOR mixing period were employed, with 32 transients for each of 16 complex (States-TPPI) t_1 increments of 123.3 μs acquired, using a recycle delay of 3.4 s between transients and 50 Hz exponential apodization in both dimensions before double Fourier transform.

Sample preparation for ssNMR

6-GH samples for ssNMR studies were prepared as pellets (~7 mg) that were either soaked in an electrolyte for 90 min or polarized for 90 min at a constant potential of -1.3 V or +1.5 V vs. Ag in a three-electrode Swagelok cell (Fig S1). Wet pellets of 6-GH (soaked/polarized) were then transferred to a P4 fritted Buchner filter (10-15 μm) and mildly washed with ~10 ml of acetonitrile under applied vacuum. Later, the dried powder was further dried in a vacuum oven at 65

^{o}C for 4 h. Samples were also prepared without the washing step by directly transferring wet pellets into vacuum oven.

RESULTS AND DISCUSSION

Pillared graphene materials are generally synthesized through a direct reaction of aqueous GO solution with alkyl diamines as pillars.[12] The amine groups react with epoxy and carboxylic groups on adjacent graphene oxide sheets and result in covalently-bridged graphene sheets.

However, owing to the reducing nature of alkyl diamines, GO sheets undergo partial and simultaneous chemical reduction and restack into graphitic particles, resulting in a biphasic material that consists of domains of both covalently-bridged and restacked graphene.[17] The obtained pillared materials are then reduced further to remove residual oxygen functionalities, improve electrical conductivity and facilitate their application in SCs. Recently, we synthesized a pillared graphene hydrogel (6-GH) through simultaneous pillaring and reduction of GO in a one-step hydrothermal process using 1,6-hexanediamine as the pillar molecule.[21] This material

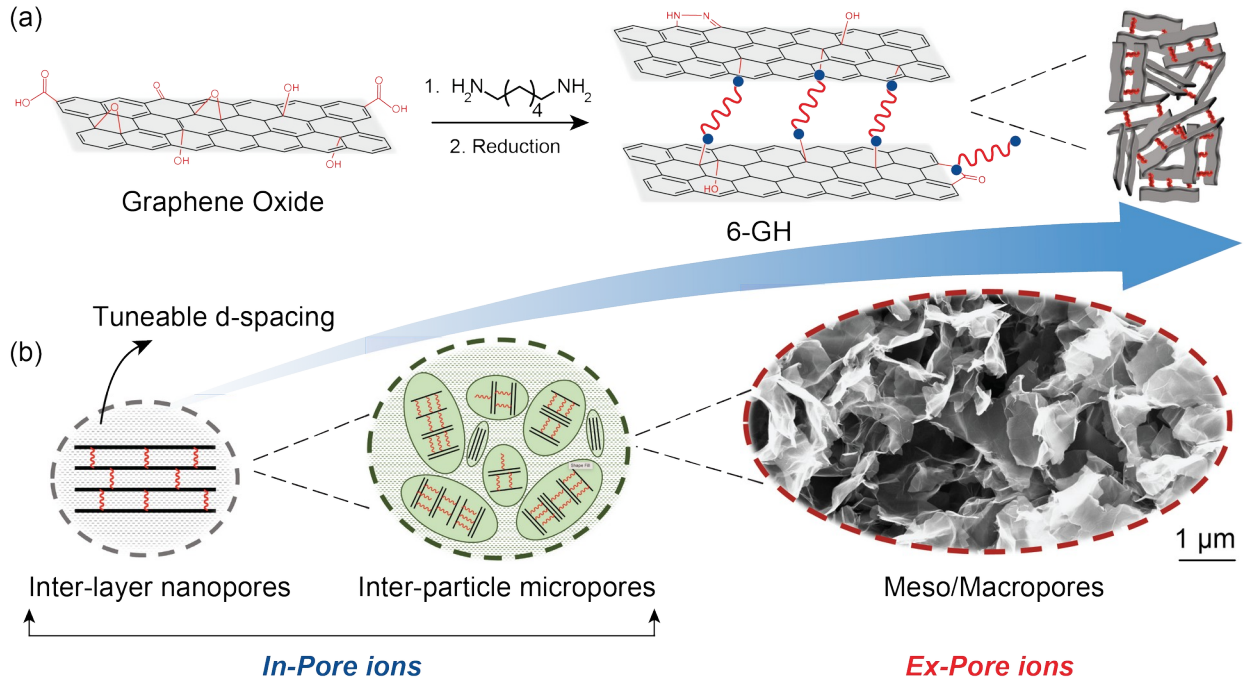

demonstrated a high specific capacitance of ~225 F/g, benefitting from an enhanced ion sorption in the synthesized 2D galleries. In order to investigate this ion-sorption through ssNMR techniques, herein, the pillar molecules were isotopically-enriched using ^{15}N-labeled 1,6-hexanediamine.

Figure 1. (a) Schematic representation of the synthesis of pillared graphene hydrogel (6-GH) using 1,6-hexanediamine as the pillar. b) Various types of porosities present in 6-GH schematically represented according to their length scales, with the meso/macro-scale porosity shown through an SEM image (right). Micro-scale depicts the biphasic nature of 6-GH with presence of both cross-linked graphene particles and restacked graphitic particles (RGO-like). Ions adsorb in the inter-layer nanopores and the inter-particular micropores (together termed as in-pore ions) whereas, the ions in meso-macro pores (termed as ex-pore ions) serve as buffer stock for the bulk electrolyte.

The synthesized 6-GH displays a 3D monolithic structure and a strong presence of both cross-linked (pillared graphene) and restacked (RGO-like) domains in the X-ray diffraction (XRD) patterns (Fig. 1b & S3). Scanning electron microscopy shows the presence of an extended 3D macroporous structure throughout the monolith (Fig. 1b). From XRD patterns, an inter-layer separation of 7.8 Å has been assigned between the graphene sheets, in line with earlier reports on diamine-pillared graphene materials.[10,12] X-ray photoelectron spectra (XPS) show that the majority of N in 6-GH occur as amines in pillars with smaller contributions from N as pyrrolic and graphitic moieties (see Fig. S4). Low temperature {^{1}H-}^{15}N CP MAS NMR spectra of 6-GH

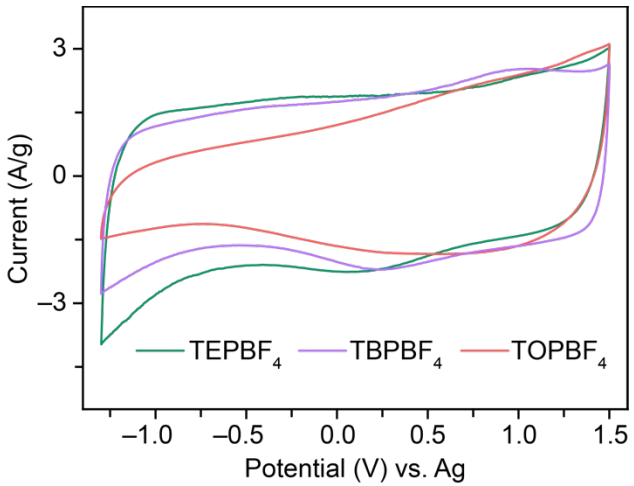

show the distinct presence of secondary amines (at $\delta\{^{15}N\}$ ~80 ppm) in 6-GH (see Fig. S5a) indicating the covalent bridging between alkyl diamines and graphene layers, as well as primary amines (at $\delta\{^{15}N\}$ ~20-50 ppm) and secondary amides, pyrrolic, pyridinic, and graphitic N (at $\delta\{^{15}N\}$ ~100-200 ppm).[38]

Figure 2. Cyclic voltammogram curves of 6-GH in $TEPBF_4$, $TBPBF_4$ and $TOPBF_4$ / acetonitrile (ACN) 1M electrolytes recorded at 20 mV/s. The increasing cation sizes from 0.69 to 0.82 and 1.12 nm for TEP^+, TBP^+ and TOP^+, respectively, result in lower currents under negative potentials.

Electrolytic ion	Diameter (nm)
Tetraethyl phosphonium (TEP^+)	0.68
Tetrabutyl phosphonium (TBP^+)	0.82
Tetraoctyl phosphonium (TOP^+)	1.12
Tetrafluoroborate (BF_4^-)	0.48

Table 1. Ion sizes of the various electrolytic salts used in this study. These values were obtained from prior reports in the literature.[40,41] They were calculated using molecular modelling approaches and verified by crystallographic measurements, correspond to ions in their un-solvated states.

6-GH was tested for its electrochemical properties through cyclic voltammetry (CV) using a family of 1M ($TAP^+BF_4^-$/ACN) electrolytes since the large NMR receptivity of ^{31}P in the cations results in an excellent probe for NMR analysis (compared to $^{14/15}N$ and ^{13}C in tetraalkylammonium ions). Alkyl phosphonium cations of varied sizes with increasing alkyl chain lengths of ethyl (TEP^+), butyl (TBP^+) and octyl (TOP^+) (Table 1) allowed for analysis of size-based ion sieving[39–41] in 6-GH. CVs were recorded at 20 mV/s after electrowetting of the electrodes during several initial cycles and the obtained curves were normalized using the weight of graphene material in the electrode (Fig. 2). CVs obtained in $TEP^+BF_4^-$/ACN, $TBP^+BF_4^-$/ACN, and $TOP^+BF_4^-$/ACN for 6-GH show similar rectangular curves for potentials higher than 0.2 V vs Ag — the initial OCV — but differ greatly for potentials lower than 0.2 V vs Ag. Since anion adsorption is recognized as a major process under positive polarization, the similarity in the curves is expected as the BF_4^- anion (with a smaller diameter than the d-spacing of 6-GH) is used in all cases. However, under negative polarization with respect to OCV, a gradual decrease in the intensity of currents can be seen with increasing cation size. Considering that TEP^+ is smaller than the inter-layer gallery spacing of 7.8 Å in 6-GH, it shows a rectangular behaviour which is consistent with a facile ion sorption within the carbon material. However, TBP^+ and TOP^+, which are, respectively, in the same range or larger than the d-spacing have increasingly limited access to the galleries and thus the CVs show a fairly symmetric deformation at negative voltages with substantial decrease in current. As a result, it turns out 6-GH's electrochemical behaviour, in such electrolytes, upon negative polarization is correlated with the cation size: the larger the

cation, the lower the current. It is noteworthy that CVs recorded using $TEPBF_4$ electrolyte displayed relatively similar curves from the 1st to 100th cycles (Fig. S6a). However, CVs using larger $TAPBF_4$ salts displayed a gradual enhancement in current in the first 100 cycles (Fig. S6b). We suspect that a gradual activation and enhancement of electrochemically active in-pore surface area may cause this gradual increase in currents for ions that experience more difficulties to access the inter-layer galleries. These electrochemical results of 6-GH in $TEP^+BF_4^-$, $TBP^+BF_4^-$, and $TOP^+BF_4^-$ /ACN thus demonstrate a sieving based on ion size versus d-spacing of a graphene-based material, and highlight 6-GH as well-suited for NMR characterization of ion sorption in inter-layer graphene galleries.

LT-MAS NMR experiments were performed on pristine and polarized 6-GH electrodes that were prepared by washing the excess electrolyte from the meso/macro pores in order to get a clearer picture of only species that are close to graphene surfaces. This washing is similar to the approach taken by Deschamps et al.[27] The scope of the work here is to analyse whether ions are only adsorbed in the inter-particle micro porosity and/or also in the inter-layer pores (Fig. 1b), and the low temperature experiments enable the sensitive detection required to probe these distinctions via NMR spectroscopy. Samples were also prepared without the washing step as a comparison. Here, the combination of ^{31}P observation and low temperature experiments qualitatively shows ion adsorption/presence in these pillared graphene materials after washing, without being obscured by signals from the bulk. Forse et al. employed polarization transfer

methods between ^{13}C-enriched porous carbon electrodes and electrolytes at room temperature for similar purposes.[42,43]

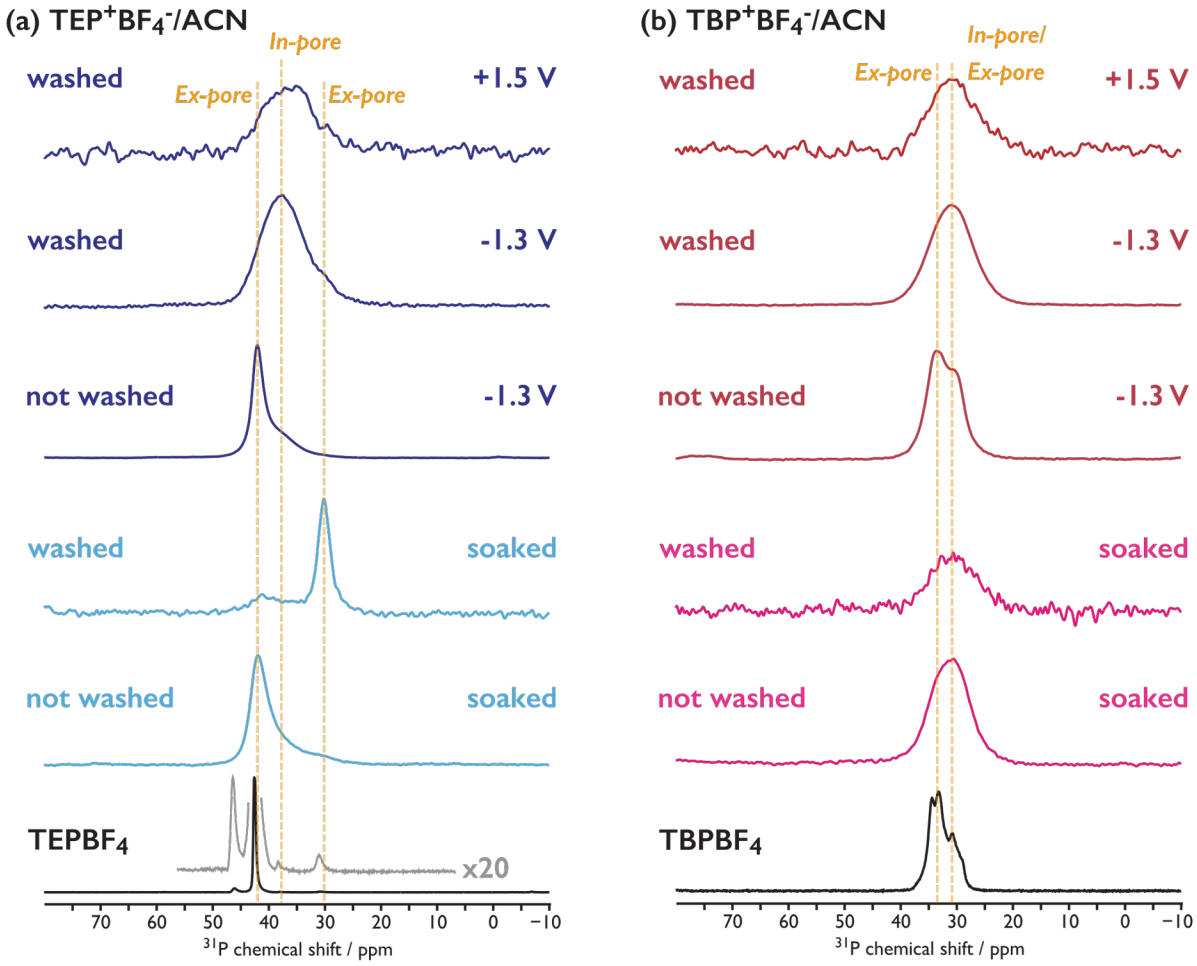

Figure 3. {^{1}H-}^{31}P LT CPMAS NMR spectra at 100 K of 6-GH electrodes with TEP^{+}BF$_4^{-}$/ACN (a) and TBP^{+}BF$_4^{-}$/ACN (b) as electrolyte, whether soaked, soaked and washed, or polarized at -1.3 V and +1.5 V vs. Ag and then washed (or not). Also given as a comparison are corresponding spectra of the bare TAPBF$_4$ salts (bottom).

The {^{1}H-}^{31}P LT CPMAS NMR spectra of 6-GH unpolarized and soaked in electrolyte and washed with ACN, shown in Fig. 3, qualitatively demonstrate that the low temperature

methodology provides good NMR signal-to-noise ratios for small amounts of remaining electrolyte, which are quite different to those of unwashed samples. Notably, the ^{31}P spectrum of 6-GH soaked in $TEP^+BF_4^-$/ACN and unwashed displays a major peak at 42 ppm with minor shoulders at lower chemical shifts (30-38 ppm). This is in stark contrast to the washed sample that shows the most intense peak at 30 ppm, with a remaining low intensity and broad contribution centred at ~38 ppm (see Fig. 3a). The observed ^{31}P spectrum of the unwashed sample is comparable to that observed for earlier work with the same electrolyte but with porous carbon electrodes and corresponds to free ex-pore (~41 ppm) and adsorbed in-pore (~34 ppm) cations, respectively.[23]

It is interesting to note that the ^{31}P peak around 42 ppm in the soaked and unwashed sample is also present in the bare salt although the resonance is less broadened. This suggests the presence of an ion-pairing effect between TEP^+ and BF_4^- in the unwashed sample (at the concentration used in this study). Interestingly, for the washed sample, this large contribution at 42 ppm is mostly removed. The remaining ^{31}P resonance appears around 30 ppm and is tentatively assigned to ex-pore TEP^+ ions that are shielded by distance from BF_4^- (possibly owing to a full solvation shell of ACN). The resonance at 38 ppm, which is clearly present in the sample polarized at -1.3 V and washed, can be attributed to adsorbed in-pore cations. The effect of the graphene ring current can clearly be seen here because of the relatively small size of the TEP^+ cations.

Unwashed 6-GH prepared with $TBP^+BF_4^-$/ACN gave a $\{^1H\text{-}\}^{31}P$ LT CPMAS NMR spectrum of similar intensity to that of unwashed $TEP^+BF_4^-$/ACN, but displayed a broad signal (see Fig. 3b) around 31-34 ppm; we note that peak intensities are discussed here as a crude approximation but the study remains qualitative. It is interesting to note that these chemical shifts are also consistent with an ion-pairing effect since they match the resonances present in the bare salt. Nevertheless, TBP^+ cations are larger, so one should expect the effect of the BF_4^- anions on the ^{31}P chemical shift to be reduced. It is also interesting to note that there is a diversity in ^{31}P chemical shift visible for both pure $TEPBF_4$ and $TBPBF_4$ (Fig. 3a inset and Fig. 3b). The pure salts are similar to organic ionic plastic crystals, with disorder leading to different ^{31}P chemical shifts.[44]

Upon washing, the resulting spectrum of 6-GH with $TBP^+BF_4^-$/ACN shows a dramatic decrease in the ^{31}P signal intensity, as could be expected; most free TBP^+ are washed away. This is not the case after the sample has been polarized to -1.3V where one can detect a large signal centred at 31 ppm, which is thus attributed to adsorbed in-pore TBP^+.

The relatively small difference in ^{31}P chemical shift between the in-pore signals (31 ppm) and free cations (34 ppm) for $TBP^+BF_4^-$/ACN could be attributed to the lesser influence of ring currents from the graphene electrode and interactions with BF_4^- anions, respectively, on the ^{31}P spins in the larger cations. Overall, this analysis shows that washing the samples is an efficient way to focus mainly on adsorbed cations. Hereafter, all discussion will hence be focused on washed samples.

After being polarized at -1.3 V vs. Ag in $TEP^+BF_4^-$/ACN (Fig. 3a), $TBP^+BF_4^-$/ACN (Fig. 3b) or $TOP^+BF_4^-$/ACN (Fig. S7), 6-GH samples exhibit a tremendous increase in the intensity of adsorbed cation signal, compared to that of the corresponding soaked sample (~50 times). This indicates, as expected, that negative polarization results in enhanced adsorption of cations. TEP^+ displays a major, broad ^{31}P signal at 38 ppm, thus corresponding to adsorbed species. The intense TBP^+ ^{31}P signal is clearly recorded at 31 ppm. Here again, this negligible shift between bulk and adsorbed species is explained by the graphene shielding effect[31] and interactions with BF_4^- anions being minimized by the lengthier alkyl chains from this cation. This interpretation is further confirmed by the absence of shift between bulk and adsorbed peaks for TOP^+ (both ~30 ppm – see Fig. S7).

Contrary to expectations, the $\{^1H-\}^{31}P$ LT CPMAS NMR spectra of 6-GH soaked with electrolyte and polarized directly to +1.5 V vs. Ag (from its pristine state) for 90 min show peaks corresponding to adsorbed cations (see Fig. 3). This could also indicate that charge diffusion upon cycling does not rely on a full anion/cation exchange or on full cation depleting mechanisms.[45] Another interpretation could be that the ions enter the inter-layer graphene galleries upon soaking 6-GH, and cations are then not fully removed with simple polarization up to +1.5 V. This presence of adsorbed cations even under positive polarization is interesting and supports our earlier impedance studies, wherein ion transport was found to depend strongly on both counter ions and co-ions.[20] The presence of adsorbed cations under positive polarization was also observed with room temperature ssNMR spectroscopy (see Fig. S5b). A comparison to

the corresponding ssNMR spectrum recorded at low temperature (Fig. 3 and Fig. S5b) demonstrates the sensitivity gains from these low temperature measurements where a worse signal-to-noise ratio was obtained at room temperature even after 25 times more accumulated scans.

Although interactions between electrolyte ions and graphene have been inferred in the above ssNMR data, no clear evidence was observed to differentiate ion sorption in the in-pore inter-particular and in-gallery 2D porosities.

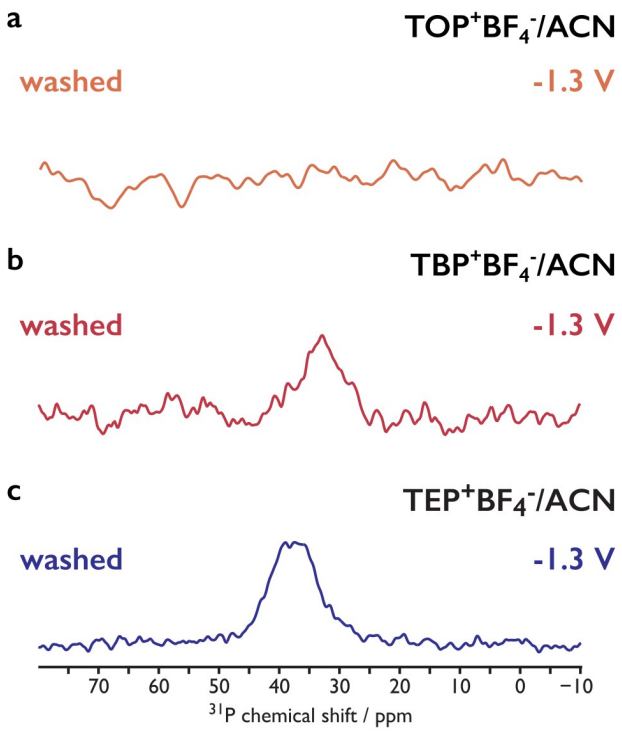

Figure 4. 1D LT CPMAS {^{15}N-}^{31}P *zf*-TEDOR NMR spectra of 6-GH electrodes after negative polarization and various electrolytes (TOP^+ (a), TBP^+ (b), and TEP^+ (c) with BF_4^-/ACN), recorded using a total of 7 ms of TEDOR recoupling.

Since single-step CP ($^{1}H \rightarrow {}^{31}P$) experiments did not provide specific information about ion sorption sites inside the interlayer space, z-filtered Transferred Echo Double Resonance (*zf*-TEDOR) was employed.[37] This experiment probes spatial proximities between heteronuclei, here ^{15}N from the pillars and ^{31}P from the cations, and can be combined with a sensitivity-enhancing $\{^{1}H\text{-}\}^{31}P$ CP step. The 1D LT CPMAS $\{^{15}N\text{-}\}^{31}P$ *zf*-TEDOR NMR spectra of the negatively polarized 6-GH samples are shown in Fig. 4. None of the non-polarized 6-GH samples soaked in the various electrolytes give a ^{31}P NMR signal using $\{^{15}N\text{-}\}^{31}P$ *zf*-TEDOR most likely due to the relative scarcity of cations in the sample that will be in close proximity of the ^{15}N-enriched organic pillars (compared to negatively polarized 6-GH in electrolyte). When 6-GH in $TEP^{+}BF_4^{-}$/ACN or $TBP^{+}BF_4^{-}$/ACN is charged to –1.3 V vs. Ag, clear ^{31}P signals from adsorbed cations are observed (see Fig. 4c and Fig 4b, respectively), revealing a proximity between these cations and nitrogen atoms in the pillars. Two phenomena could lead to the above observations: (i) TEP^{+} and TBP^{+} cations may enter the inter-layer spaces in 6-GH under negative polarization and be in sufficiently close proximity to the pillar molecules; (ii) relatively more cations may enter the inter-particular porosity under negative polarization, leading to shorter cation-pillar distances on average than when the sample is only soaked. To distinguish scenario (i), an electrolyte with cations of diameter larger than the inter-gallery d-spacing of 6-GH was employed; $TOP^{+}BF_4^{-}$/ACN contains cations with a diameter of ~ 11.2 Å (cf. 7.8 Å for the d-spacing).[40] Although $\{^{1}H\text{-}\}^{31}P$ LT CPMAS NMR experiments of 6-GH in $TOP^{+}BF_4^{-}$/ACN provide good signal-to-noise (see Fig. S7), no signal is observed for the $\{^{15}N\text{-}\}^{31}P$ *zf*-TEDOR

experiment (see Fig. 4a and Fig. S8). This suggests that there is not a sufficient amount of TOP^+ ions in proximity to ^{15}N from the electrode and thus that the large TOP^+ ions do not enter into the graphene galleries of 6-GH. This corroborates the conclusions from the electrochemical measurements (*vide supra*).

To ensure that the absence of $\{^{15}N\text{-}\}^{31}P$ *zf*-TEDOR signal for 6-GH with $TOP^+BF_4^-$/ACN is not due to the larger distance between ^{31}P and ^{15}N because of the octyl chains of TOP, a reference experiment was performed. A guanosine derivative was chosen (Guanosine-$^{15}N_5$ 5'-monophosphate sodium salt solution, GMP) that bears a variety of ^{31}P–^{15}N distances, from approximately 6 to 11 Å (cf. TOP^+ radius of <10 Å). From a 2D LT CPMAS ^{15}N-^{31}P *zf*-TEDOR NMR spectrum (using the same TEDOR recoupling time as for the experiments on 6-GH) for diluted (25 mM) GMP, cross peaks for even the furthest ^{15}N-^{31}P spin pairs are observed (see Fig. S9). Moreover, longer TEDOR recoupling times (up to 20 ms) were also attempted for 6-GH in $TOP^+BF_4^-$/ACN, with still no observed signal (see Fig. S8). This rules out the longer alkyl chain length of TOP^+ as the reason for absence of $\{^{15}N\text{-}\}^{31}P$ *zf*-TEDOR signal. Therefore, this shows that TOP^+ cations do not enter the graphene galleries as expected considering their size and, by extension, confirms that the NMR signal observed for $\{^{15}N\text{-}\}^{31}P$ *zf*-TEDOR experiments of 6-GH with $TEP^+BF_4^-$/ACN and $TBP^+BF_4^-$/ACN does indeed come from cations confined between the pillared layers.

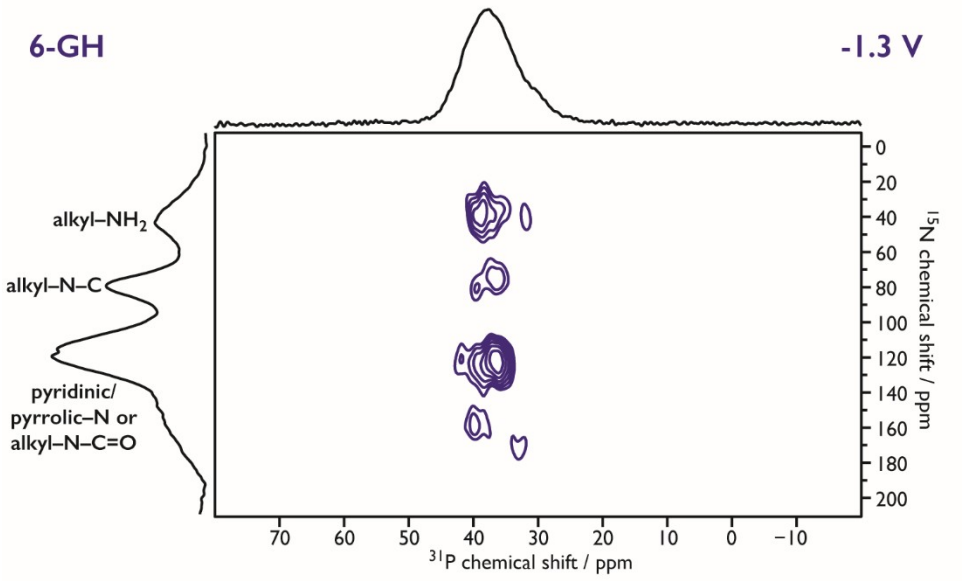

Figure 5. 2D LT CPMAS ^{15}N-^{31}P *zf*-TEDOR NMR spectrum of 6-GH electrodes with negative polarization and TEP^{+}BF$_4^{-}$/ACN electrolyte, recorded using a total of 7 ms of TEDOR recoupling.

The proximity between electrolyte and the pillars is only detected here through {^{15}N-}^{31}P *zf*-TEDOR experiments when there is a sufficient number of dipolar (through-space) coupled nuclei, as is the case when the electrolyte can enter high-surface area pillared graphene interlayers. To gain further information on specific interaction sites within the graphene galleries, a 2D LT CPMAS ^{15}N-^{31}P *zf*-TEDOR NMR spectrum of 6-GH with TEP^{+}BF$_4^{-}$/ACN and negative polarization was acquired, and is shown in Fig. 5. It can be seen that ^{31}P spins from the electrolyte cations correlate to ^{15}N in a variety of different environments found in the pillared graphene material: free amines, N in α of the graphene sheet, N from amides, and N from pyridinic or pyrrolic moieties. Moreover, it appears that different ^{15}N environments correlate

more or less strongly to two particular ^{31}P chemical shifts (evidenced by the relative intensity of the contours and via cross-sectional slices (see Fig. S11)), at 39 and 36 ppm. Amines and amides that could be expected near to the edges of the graphene sheets correlate to the higher-shifted ^{31}P resonance at 39 ppm, which could be expected if cations near the edges were then less affected by ring currents in the graphene.[31] Conversely, cations in the centre of the sheets would be most affected by the ring currents. Indeed, the ^{31}P resonance showing the lower shift, at 36 ppm, correlates most strongly to ^{15}N-containing moieties that are expected to covalently link the graphene sheets together (N in α of the graphene and pyridinic- or pyrrolic-N). This tentative assignment indicates that the broadness (~ 9 ppm) of the ^{31}P NMR signal from adsorbed TEP^+ cations is at least partly due to varied positions of the electrolyte cations with respect to the pillared graphene electrode.

CONCLUSIONS

In summary, this study presents low temperature MAS NMR spectroscopy as an efficient and powerful technique to investigate electrolytic ion sorption in pillared graphene hydrogel electrodes suitable for use in supercapacitors. Extensive analysis using electrolytic cations of varied sizes and under different bias potentials has revealed that ions enter inter-layer 2D galleries in 6-GH when chosen appropriately. Specifically, when 6-GH is used in combination with a cation of larger diameter than the d-spacing, nuclear polarization transfer is not observed between the electrolyte cations and the pillars as these ions are too big to enter the 2D galleries.

Only when 6-GH is used in combination with a cation smaller than the d-spacing do cations enter the graphene galleries. Nuclear polarization transfer between cations inside the galleries and isotopically-enriched marker nuclei from the pillars reveals that the cations can be found in various chemical environments within these graphene galleries. Overall, LT MAS ssNMR offers a new atomic-scale method to probe ion-sorption in SCs and similar devices, presenting enormous potential for understanding dynamic mechanisms, thus leading to further improved energy storage materials.

ASSOCIATED CONTENT

Supporting Information

Material characterization, instrumentation details, ssNMR data acquisition protocols, control experiments on guanosine derivates are included in supporting information file.

AUTHOR INFORMATION

Corresponding Author

Florence Duclairoir: florence.duclairoir@cea.fr

Gaël De Paëpe: gael.depaepe@cea.fr

Present Addresses

Department of Chemical Engineering, University of Manchester, Manchester M13 9PL, United Kingdom

ǂ Department of Chemistry, Massachusetts Institute of Technology, Cambridge, MA 02139, United States

Author Contributions

DL, HB, FD and GDP proposed and led the project. DL, HB, SP and CM performed experiments. PLT, PS and LD helped interpret results. The manuscript was written through contributions of all authors. All authors have given approval to the final version of the manuscript. †These authors contributed equally.

Funding Sources

Authors acknowledge funding support by CEA and by the French National Research Agency (SUGGEST-ANR-15-CE05-0022, ANR-12-BS08-0016-01, ANR-11-LABX-0003-01 and RTB) as well as the European Research Council (ERC-CoG- 2015, No. 682895).

ACKNOWLEDGEMENT

Authors appreciate the access to mutualized equipment provided by PFNC Nano-characterization Minatec platforms.

Present address: #DL: Department of Chemical Engineering, University of Manchester, Manchester M13 9PL, United Kingdom.

Present address: ǂHB: Department of Chemistry and Biochemistry, The University of Texas, El Paso, Texas, USA.

REFERENCES

(1) Simon, P.; Gogotsi, Y. Materials for Electrochemical Capacitors. *Nature Mater* **2008**, *7* (11), 845–854. https://doi.org/10.1038/nmat2297.

(2) Béguin, F.; Presser, V.; Balducci, A.; Frackowiak, E. Carbons and Electrolytes for Advanced Supercapacitors. *Advanced Materials* **2014**, *26* (14), 2219–2251. https://doi.org/10.1002/adma.201304137.

(3) Miller, J. R.; Simon, P. Electrochemical Capacitors for Energy Management. *Science* **2008**, *321* (5889), 651. https://doi.org/10.1126/science.1158736.

(4) Chmiola, J.; Yushin, G.; Gogotsi, Y.; Portet, C.; Simon, P.; Taberna, P. L. Anomalous Increase in Carbon Capacitance at Pore Sizes Less Than 1 Nanometer. *Science* **2006**, *313* (5794), 1760. https://doi.org/10.1126/science.1132195.

(5) Pech, D.; Brunet, M.; Durou, H.; Huang, P.; Mochalin, V.; Gogotsi, Y.; Taberna, P.-L.; Simon, P. Ultrahigh-Power Micrometre-Sized Supercapacitors Based on Onion-like Carbon. *Nature Nanotechnology* **2010**, *5* (9), 651–654. https://doi.org/10.1038/nnano.2010.162.

(6) Frackowiak, E.; Metenier, K.; Bertagna, V.; Beguin, F. Supercapacitor Electrodes from Multiwalled Carbon Nanotubes. *Appl. Phys. Lett.* **2000**, *77* (15), 2421–2423. https://doi.org/10.1063/1.1290146.

(7) Chen, J.; Li, C.; Shi, G. Graphene Materials for Electrochemical Capacitors. *J. Phys. Chem. Lett.* **2013**, *4* (8), 1244–1253. https://doi.org/10.1021/jz400160k.

(8) Xia, J.; Chen, F.; Li, J.; Tao, N. Measurement of the Quantum Capacitance of Graphene. *Nature Nanotechnology* **2009**, *4* (8), 505–509. https://doi.org/10.1038/nnano.2009.177.

(9) Stoller, M. D.; Park, S.; Zhu, Y.; An, J.; Ruoff, R. S. Graphene-Based Ultracapacitors. *Nano Lett.* **2008**, *8* (10), 3498–3502. https://doi.org/10.1021/nl802558y.

(10) Bourlinos, A. B.; Gournis, D.; Petridis, D.; Szabó, T.; Szeri, A.; Dékány, I. Graphite Oxide: Chemical Reduction to Graphite and Surface Modification with Primary Aliphatic Amines and Amino Acids. *Langmuir* **2003**, *19* (15), 6050–6055. https://doi.org/10.1021/la026525h.

(11) Matsuo, Y.; Higashika, S.; Kimura, K.; Miyamoto, Y.; Fukutsuka, T.; Sugie, Y. Synthesis of Polyaniline-Intercalated Layered Materials via Exchange Reaction. *Journal of Materials Chemistry* **2002**, *12* (5), 1592–1596. https://doi.org/10.1039/B107436A.

(12) Herrera-Alonso, M.; Abdala, A. A.; McAllister, M. J.; Aksay, I. A.; Prud'homme, R. K. Intercalation and Stitching of Graphite Oxide with Diaminoalkanes. *Langmuir* **2007**, *23* (21), 10644–10649. https://doi.org/10.1021/la0633839.

(13) Garberoglio, G.; Pugno, N. M.; Taioli, S. Gas Adsorption and Separation in Realistic and Idealized Frameworks of Organic Pillared Graphene: A Comparative Study. *J. Phys. Chem. C* **2015**, *119* (4), 1980–1987. https://doi.org/10.1021/jp511953p.

(14) Jiang, L.; Sheng, L.; Long, C.; Wei, T.; Fan, Z. Functional Pillared Graphene Frameworks for Ultrahigh Volumetric Performance Supercapacitors. *Advanced Energy Materials* **2015**, *5* (15), 1500771–n/a. https://doi.org/10.1002/aenm.201500771.

(15) Sun, J.; Morales-Lara, F.; Klechikov, A.; Talyzin, A. V.; Baburin, I. A.; Seifert, G.; Cardano, F.; Baldrighi, M.; Frasconi, M.; Giordani, S. Porous Graphite Oxide Pillared with Tetrapod-Shaped Molecules. *Carbon* **2017**, *120*, 145–156. https://doi.org/10.1016/j.carbon.2017.05.007.

(16) Lee, K.; Yoon, Y.; Cho, Y.; Lee, S. M.; Shin, Y.; Lee, H.; Lee, H. Tunable Sub-Nanopores of Graphene Flake Interlayers with Conductive Molecular Linkers for Supercapacitors. *ACS Nano* **2016**, *10* (7), 6799–6807. https://doi.org/10.1021/acsnano.6b02415.

(17) Banda, H.; Daffos, B.; Périé, S.; Chenavier, Y.; Dubois, L.; Aradilla, D.; Pouget, S.; Simon, P.; Crosnier, O.; Taberna, P.-L.; Duclairoir, F. Ion Sieving Effects in Chemically Tuned Pillared Graphene Materials for Electrochemical Capacitors. *Chem. Mater.* **2018**, *30* (9), 3040–3047. https://doi.org/10.1021/acs.chemmater.8b00759.

(18) Yuan, K.; Xu, Y.; Uihlein, J.; Brunklaus, G.; Shi, L.; Heiderhoff, R.; Que, M.; Forster, M.; Chassé, T.; Pichler, T.; Riedl, T.; Chen, Y.; Scherf, U. Straightforward Generation of Pillared, Microporous Graphene Frameworks for Use in Supercapacitors. *Adv. Mater.* **2015**, *27* (42), 6714–6721. https://doi.org/10.1002/adma.201503390.

(19) Hung, W.-S.; Tsou, C.-H.; De Guzman, M.; An, Q.-F.; Liu, Y.-L.; Zhang, Y.-M.; Hu, C.-C.; Lee, K.-R.; Lai, J.-Y. Cross-Linking with Diamine Monomers To Prepare Composite Graphene Oxide-Framework Membranes with Varying d-Spacing. *Chem. Mater.* **2014**, *26* (9), 2983–2990. https://doi.org/10.1021/cm5007873.

(20) Banda, H.; Périé, S.; Daffos, B.; Dubois, L.; Crosnier, O.; Simon, P.; Taberna, P.-L.; Duclairoir, F. Investigation of Ion Transport in Chemically Tuned Pillared Graphene Materials through Electrochemical Impedance Analysis. *Electrochimica Acta* **2019**, 296, 882-890. https://doi.org/10.1016/j.electacta.2018.11.122.

(21) Banda, H.; Périé, S.; Daffos, B.; Taberna, P.-L.; Dubois, L.; Crosnier, O.; Simon, P.; Lee, D.; De Paëpe, G.; Duclairoir, F. Sparsely Pillared Graphene Materials for High-Performance Supercapacitors: Improving Ion Transport and Storage Capacity. *ACS Nano* **2019**, *13* (2), 1443–1453. https://doi.org/10.1021/acsnano.8b07102.

(22) Wang, H.; Forse, A. C.; Griffin, J. M.; Trease, N. M.; Trognko, L.; Taberna, P.-L.; Simon, P.; Grey, C. P. In Situ NMR Spectroscopy of Supercapacitors: Insight into the Charge Storage Mechanism. *J. Am. Chem. Soc.* **2013**, *135* (50), 18968–18980. https://doi.org/10.1021/ja410287s.

(23) Griffin, J. M.; Forse, A. C.; Tsai, W.-Y.; Taberna, P.-L.; Simon, P.; Grey, C. P. In Situ NMR and Electrochemical Quartz Crystal Microbalance Techniques Reveal the Structure of the Electrical Double Layer in Supercapacitors. *Nature Materials* **2015**, *14* (8), 812–819. https://doi.org/10.1038/nmat4318.

(24) Wang, H.; Köster, T. K.-J.; Trease, N. M.; Ségalini, J.; Taberna, P.-L.; Simon, P.; Gogotsi, Y.; Grey, C. P. Real-Time NMR Studies of Electrochemical Double-Layer Capacitors. *J. Am. Chem. Soc.* **2011**, *133* (48), 19270–19273. https://doi.org/10.1021/ja2072115.

(25) Oukali, G.; Salager, E.; Ammar, M. R.; Dutoit, C.-E.; Sarou-Kanian, V.; Simon, P.; Raymundo-Piñero, E.; Deschamps, M. In Situ Magnetic Resonance Imaging of a Complete Supercapacitor Giving Additional Insight on the Role of Nanopores. *ACS Nano* **2019**, *13* (11), 12810–12815. https://doi.org/10.1021/acsnano.9b04998.

(26) Deschamps, M.; Cadars, S.; Gilbert, E.; Azaïs, P.; Raymundo-Pinero, E.; Béguin, F.; Massiot, D. A Solid-State NMR Study of C70: A Model Molecule for Amorphous Carbons. *Solid State Nuclear Magnetic Resonance* **2012**, *42*, 81–86. https://doi.org/10.1016/j.ssnmr.2012.01.001.

(27) Deschamps, M.; Gilbert, E.; Azais, P.; Raymundo-Piñero, E.; Ammar, M. R.; Simon, P.; Massiot, D.; Béguin, F. Exploring Electrolyte Organization in Supercapacitor Electrodes with Solid-State NMR. *Nature Materials* **2013**, *12* (4), 351–358. https://doi.org/10.1038/nmat3567.

(28) Fulik, N.; Hippauf, F.; Leistenschneider, D.; Paasch, S.; Kaskel, S.; Brunner, E.; Borchardt, L. Electrolyte Mobility in Supercapacitor Electrodes – Solid State NMR Studies on Hierarchical and Narrow Pore Sized Carbons. *Energy Storage Materials* **2018**, *12*, 183–190. https://doi.org/10.1016/j.ensm.2017.12.008.

(29) Borchardt, L.; Oschatz, M.; Paasch, S.; Kaskel, S.; Brunner, E. Interaction of Electrolyte Molecules with Carbon Materials of Well-Defined Porosity: Characterization by Solid-State NMR Spectroscopy. *Phys. Chem. Chem. Phys.* **2013**, *15* (36), 15177–15184. https://doi.org/10.1039/C3CP52283K.

(30) Forse, A. C.; Griffin, J. M.; Merlet, C.; Bayley, P. M.; Wang, H.; Simon, P.; Grey, C. P. NMR Study of Ion Dynamics and Charge Storage in Ionic Liquid Supercapacitors. *J. Am. Chem. Soc.* **2015**, *137* (22), 7231–7242. https://doi.org/10.1021/jacs.5b03958.

(31) Forse, A. C.; Griffin, J. M.; Presser, V.; Gogotsi, Y.; Grey, C. P. Ring Current Effects: Factors Affecting the NMR Chemical Shift of Molecules Adsorbed on Porous Carbons. *J. Phys. Chem. C* **2014**, *118* (14), 7508–7514. https://doi.org/10.1021/jp502387x.

(32) Forse, A. C.; Griffin, J. M.; Merlet, C.; Carretero-Gonzalez, J.; Raji, A.-R. O.; Trease, N. M.; Grey, C. P. Direct Observation of Ion Dynamics in Supercapacitor Electrodes Using in Situ Diffusion NMR Spectroscopy. *Nature Energy* **2017**, *2* (3), 16216. https://doi.org/10.1038/nenergy.2016.216.

(33) Forse, A. C.; Merlet, C.; Griffin, J. M.; Grey, C. P. New Perspectives on the Charging Mechanisms of Supercapacitors. *J. Am. Chem. Soc.* **2016**, *138* (18), 5731–5744. https://doi.org/10.1021/jacs.6b02115.

(34) Li, K.; Bo, Z.; Yan, J.; Cen, K. Solid-State NMR Study of Ion Adsorption and Charge Storage in Graphene Film Supercapacitor Electrodes. *Scientific Reports* **2016**, *6* (1), 39689. https://doi.org/10.1038/srep39689.

(35) Svirinovsky-Arbeli, A.; Rosenberg, D.; Krotkov, D.; Damari, R.; Kundu, K.; Feintuch, A.; Houben, L.; Fleischer, S.; Leskes, M. The Effects of Sample Conductivity on the Efficacy of Dynamic Nuclear Polarization for Sensitivity Enhancement in Solid State NMR Spectroscopy. *Solid State Nuclear Magnetic Resonance* **2019**, *99*, 7–14. https://doi.org/10.1016/j.ssnmr.2019.02.003.

(36) Thurber, K. R.; Tycko, R. Measurement of Sample Temperatures under Magic-Angle Spinning from the Chemical Shift and Spin-Lattice Relaxation Rate of 79Br in KBr Powder. *Journal of Magnetic Resonance* **2009**, *196* (1), 84–87. https://doi.org/10.1016/j.jmr.2008.09.019.

(37) Jaroniec, C. P.; Filip, C.; Griffin, R. G. 3D TEDOR NMR Experiments for the Simultaneous Measurement of Multiple Carbon−Nitrogen Distances in Uniformly 13C,15N-Labeled Solids. *J. Am. Chem. Soc.* **2002**, *124* (36), 10728–10742. https://doi.org/10.1021/ja026385y.

(38) Kim, G.; Lee, J.; Liu, T.; Grey, C. P. Characterizing Nitrogen Sites in Nitrogen-Doped Reduced Graphene Oxide: A Combined Solid-State 15N NMR, XPS, and DFT Approach. *J. Phys. Chem. C* **2021**, *125* (19), 10558–10564. https://doi.org/10.1021/acs.jpcc.1c02669.

(39) Eliad, L.; Salitra, G.; Soffer, A.; Aurbach, D. Ion Sieving Effects in the Electrical Double Layer of Porous Carbon Electrodes: Estimating Effective Ion Size in Electrolytic Solutions. *J. Phys. Chem. B* **2001**, *105* (29), 6880–6887. https://doi.org/10.1021/jp010086y.

(40) Levi, M. D.; Levy, N.; Sigalov, S.; Salitra, G.; Aurbach, D.; Maier, J. Electrochemical Quartz Crystal Microbalance (EQCM) Studies of Ions and Solvents Insertion into Highly Porous Activated Carbons. *J. Am. Chem. Soc.* **2010**, *132* (38), 13220–13222. https://doi.org/10.1021/ja104391g.

(41) Mysyk, R.; Raymundo-Piñero, E.; Pernak, J.; Béguin, F. Confinement of Symmetric Tetraalkylammonium Ions in Nanoporous Carbon Electrodes of Electric Double-Layer Capacitors. *J. Phys. Chem. C* **2009**, *113* (30), 13443–13449. https://doi.org/10.1021/jp901539h.

(42) Forse, A. C.; Griffin, J. M.; Grey, C. P. Selective Observation of Charge Storing Ions in Supercapacitor Electrode Materials. *Solid State Nuclear Magnetic Resonance* **2018**, *89*, 45–49. https://doi.org/10.1016/j.ssnmr.2017.10.003.

(43) Forse, A. C.; Griffin, J. M.; Wang, H.; Trease, N. M.; Presser, V.; Gogotsi, Y.; Simon, P.; Grey, C. P. Nuclear Magnetic Resonance Study of Ion Adsorption on Microporous Carbide-Derived Carbon. *Phys. Chem. Chem. Phys.* **2013**, *15* (20), 7722–7730. https://doi.org/10.1039/C3CP51210J.

(44) Armel, V.; Velayutham, D.; Sun, J.; Howlett, P. C.; Forsyth, M.; MacFarlane, D. R.; Pringle, J. M. Ionic Liquids and Organic Ionic Plastic Crystals Utilizing Small Phosphonium Cations. *J. Mater. Chem.* **2011**, *21* (21), 7640–7650. https://doi.org/10.1039/C1JM10417A.

(45) Griffin, J. M.; Forse, A. C.; Wang, H.; Trease, N. M.; Taberna, P.-L.; Simon, P.; Grey, C. P. Ion Counting in Supercapacitor Electrodes Using NMR Spectroscopy. *Faraday Discuss.* **2014**, *176* (0), 49–68. https://doi.org/10.1039/C4FD00138A.

Table of contents graphic

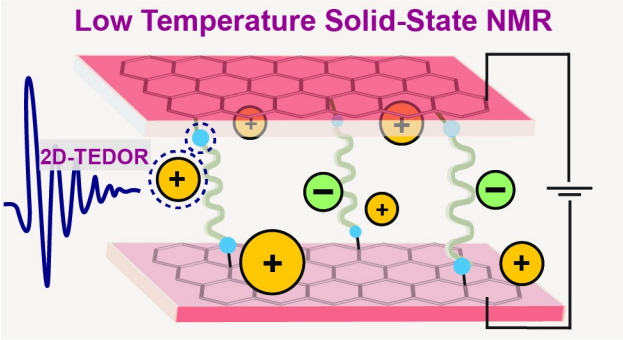

Low temperature solid-state nuclear magnetic resonance enables direct observation of electrolytic ions in between two-dimensional graphene layers.